Soft Matter

Accepted Manuscript

ROYAL SOCIETY OF CHEMISTRY

www.rsc.org/softmatter

Controlled Gelation of Poly(3-alkylthiophene)s in Bulk and in Thin-Films using Low Volatility Solvent/Poor-Solvent Mixtures

Gregory M. Newbloom[‡], *Pablo de la Iglesia*[‡] *and Lilo D. Pozzo**

Department of Chemical Engineering, University of Washington, Box 351750, Seattle, Washington, 98195-1750, United States

* Email: dpozzo@u.washington.edu. [‡] These authors contributed equally to this work.

TOC GRAPHIC:

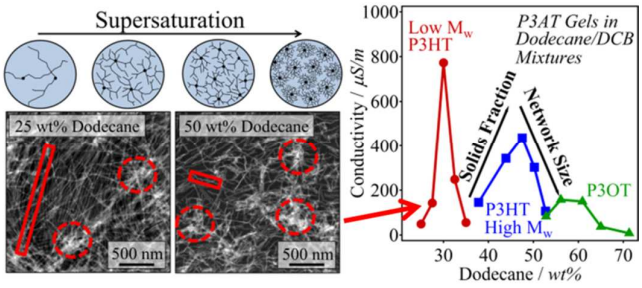

Controlled Gelation of Poly(3-alkylthiophene)s in Bulk and in Thin-Films using Low Volatility Solvent/Poor-Solvent Mixtures

Gregory M. Newbloom[‡], *Pablo de la Iglesia*[‡] *and Lilo D. Pozzo**

Department of Chemical Engineering, University of Washington, Box 351750, Seattle, Washington, 98195-1750, United States

* Email: dpozzo@u.washington.edu. [‡] These authors contributed equally to this work.

ABSTRACT:

Low volatility solvent/non-solvent mixtures were utilized to engineer the structure of poly(3-alkylthiophene) (P3AT) organogels. The ratio of solvent to poor-solvent was manipulated to systematically control the kinetics of self-assembly. Specific solvent mixtures were utilized to produce similar gelation kinetics with polymers of differing alkyl chain length. Simultaneous small angle neutron scattering (SANS) and dielectric spectroscopy was used to probe the structure and the electronic properties of isothermally self-assembled P3ATs. It was determined that alkyl chain length has a dominant effect on the relationship between fiber development and conductivity. Furthermore, using transmission electron microscopy (TEM) and SANS we demonstrate that, for P3HT organogels, lower poor-solvent content leads to fewer fibers with larger nucleation centers while higher poor-solvent amounts results in more fibers and nucleation centers that are smaller and more abundant. This leads to opposing effects in terms of the contribution of the solvent quality to the electrical conductivity. An optimum in conductivity is

found at different amounts of poor-solvent for each type of polymer. It is also shown that low volatility solvent mixtures allow for the formation of thermoreversible conjugated polymer organogels in thin-films at room temperature. This work highlights the potential to engineer the structure of conjugated polymer organogels while enabling the use of interconnected gel structures in thin-film organic electronic devices.

KEYWORDS: Conjugated Polymer, Gelation, Poly(3-alkylthiophene), Network Structure, Conductivity, Solvent Mixture

INTRODUCTION:

An interconnected network structure is ideal for several organic electronic devices, including photovoltaics and field effect transistors. In organic photovoltaics (OPVs), visible light generates electron-hole pairs in the photoactive layer which must be separated and transported through a bicontinuous, interconnected network structure towards the respective electrodes.[1, 2] In organic field effect transistors (OFETs), charges are injected into an interconnected network structure and must be transported to the electrodes.[3, 4] High performance organic electronics utilize carefully engineered nanoscale phase interconnectivity to maximize device efficiency and performance.[2, 5]

One route towards engineering network structures is the controlled gelation of conjugated polymers. Gelation is a common phenomenon amongst conjugated polymers where strong inter-chain aggregation or crystallization can result in the formation high aspect ratio fibers. [3, 4, 6-20] Varying self-assembly conditions has also been shown to modify the structure and properties of gels so that they could be designed for specific organic electronic applications.[11, 17, 19] Recently, features such as the size and crystallinity of fibers as well as the extent of branching and the

orientation of the fiber network have been characterized and shown to increase conductivity.[4, 11, 12, 21] Furthermore, it is also known that thin-films made from organogels produce higher charge mobility when compared to films cast from polymer solutions.[4, 9]

Unfortunately, the same connectivity that enhances charge transport also increases elasticity, making it difficult to coat uniform films while maintaining an intact structure.[7, 22, 23] In fact, gelation is also attributed to poor device performance in spite of conjugated polymer gels having a nearly "ideal" structure for active layers.[9, 22] This has led to the development of numerous methodologies to produce uniform coatings from gels. Huang and coworkers designed a freeze-dry coating method for poly(3-hexylthiophene) (P3HT) where a volatile solvent is sublimed under vacuum after gelation is induced by freezing.[7] Kim and coworkers developed a method that involved the sonication of a pre-formed gel prior to coating.[24] Richards and coworkers developed a coating method that involved ultrasound fragmentation in an aqueous dispersion with a stabilizing surfactant (i.e. emulsification).[23] All of these organogel coating methods have yielded promising results for organic electronics but each have issues that can damage the interconnected structure or introduce insulating molecules.

In this study, we present a facile route towards controlling poly(3-alkylthiophene) (P3AT) gelation while allowing for the formation of uniform thin-film gels at room temperature. We utilize low volatility solvent/poor-solvent mixtures to control supersaturation (i.e. driving force for gelation) while reducing the influence of solvent evaporation effects. The structure of the gels is characterized using scanning transmission electron microscopy (sTEM) and small angle neutron scattering (SANS). The mechanical and electrical properties of the gels are also measured using oscillatory rheology and dielectric spectroscopy. We demonstrate that changes in both alkyl chain length and supersaturation are effective means for the modification of structure

and properties. These results represent a step forward towards controlling the self-assembly of conjugated polymer gels as well as their ultimate application in thin-film electronic devices.

EXPERIMENTAL METHODS:

Materials. Two lots of regioregular poly(3-hexylthiophene) (P3HT), one lot of regioregular poly(3-octylthiophene) (P3OT) and one lot of regioregular poly(3-dodecylthiophene) (P3DDT) were used as received from Rieke Metals (Lincoln, NE). The molecular weight (M_w^{chain}), polydispersity index (PDI) and regioregularity (*RR*) for all of these polymers is shown in Table 1. The average contour length (L_c) of the polymer is calculated using Equation 1 and listed in Table 1.

$$L_c = \frac{M_w^{chain}}{M_w^{monomer}} \cdot L_{monomer} \quad (1)$$

The molecular weight of a monomer unit ($M_w^{monomer}$) is 166.3 g/mol for P3HT, 194.3 g/mol for P3OT and 250.4 g/mol for P3DDT while the length of a single monomer unit ($L_{monomer}$) is constant at 1.9 Å.[25, 26]

Table 1. Properties of poly(3-alkylthiophene)s including molecular weight (M_w^{chain}), polydispersity index (PDI), regioregularity (*RR*) and contour length (L_c).

	Type	**Lot #**	M_w^{chain} **(g/mol)**	**PDI**	***RR***	L_c **(nm)**
P3HT (Low M_w)	Sepiolid P200	2010-A6-7	21,000	1.6	95%	24.3 nm
P3HT (High M_w)	4002-E	PTL 12-03	53,000	2.3	92%	61.2 nm
P3OT	4003-E	PTL 11-39	83,000	1.9	91%	82.0 nm
P3DDT	4005-E	BS 14-44	51,000	1.8	92%	39.1 nm

Hydrogenated solvents 1,2-dichlorobenzene (DCB) and n-dodecane were purchased from Sigma-Aldrich (St. Louis, MO) and used as received. Deuterated solvents were used to decrease the incoherent scattering background and increase the scattering contrast in SANS and USANS experiments. D4-1,2-dichlorobenzene (D > 99%) was purchased from Cambridge Isotopes (Tewksbury, MA) and D26-Dodecane (D > 98%) was purchased from Sigma-Aldrich. Both were used as received.

Sample Preparation. All samples were prepared by adding 30 mg/mL P3AT to a mixture of 1,2-dichlorobenzene and dodecane. Samples were then heated above 80 ºC until all visible signs of polymer powder (black) had disappeared and a bright orange solution remained. All solvent mixture percentages in this work are by weight.

Neutron Scattering. Small Angle Neutron Scattering (SANS) and Ultra-Small Angle Neutron Scattering (USANS) experiments were performed at the National Institute of Standards and Technology Center for Neutron Research (NIST CNR) in Gaithersburg, MD. SANS measurements were performed on the NG3 beamline at three detector positions, for equilibrium samples, to obtain the scattering intensity, *I(q)*, over a wide *q*-range ($0.002 < q$ (Å^{-1}) < 0.4), while kinetic measurements (e.g. dielectric-SANS) used only two detector positions for a more limited *q*-range with higher flux ($0.006 < q$ (Å^{-1}) < 0.4).[27] The total scattering was normalized to the incident beam flux, corrected for empty cell scattering and 2D profiles were then converted to 1D profiles using standard methods.[28]

Equilibrium samples were measured in 1 mm pathlength demountable cells with quartz windows. Kinetic experiments simultaneously measuring AC dielectric properties and SANS (e.g. dielectric-SANS) were performed in using electrically insulated demountable cell with a 1 mm pathlength and stainless steel windows also serving as electrodes. More details regarding

this sample environment are found elsewhere.[12] Sample cells were loaded with a hot polymer solution (~ 80 °C) before being rapidly quenched (> 10 °C/min) in the beamline to experimental temperatures. Experiments were started when samples reached experimental temperatures as judged by an identical cell that was filled with ethylene glycol that was in the same temperature control block. In line with recent work, samples were run twice at different detector distances, reduced to 1D profiles and then stitched together based on the elapsed time.[12] Point-by-point matching was utilized to associate the dielectric and SANS data. USANS measurements were performed on the BT5 perfect crystal diffractometer extending the q-range to 5×10^{-5} Å^{-1} for equilibrium organogel samples. The data was reduced and desmeared using Igor-based macros developed by NIST.[29] All model fitting was performed using DANSE SASView software.[30]

Dielectric Spectroscopy. AC dielectric spectroscopy measurements were performed using an Agilent e4980a LCR Meter. A perturbation voltage of 600 mV, within the linear impedance response range, and a frequency range of 20 Hz – 2 MHz were used for all samples.[11, 12] Reported conductivities were calculated at a frequency of 2 kHz and all measurements were performed between stainless steel plates. No chemical dopants were added to any of the reported samples to enhance their conductive properties. Therefore, all conductivity values result from the transport of intrinsic charge carriers in the semiconductors.

Rheology. Oscillatory rheology measurements were performed on an Anton Paar MCR 301 stress controlled rheometer using a 25 mm parallel plate geometry. Unless otherwise stated, a frequency of 1 Hz, 0.4 mm gap and 0.25% perturbation strain (in the linear viscoelastic regime for P3HT gels), were used for all measurements.[11, 12] A fully dissolved polymer solution (~ 80 °C) was loaded into the pre-heated (40 °C) sample gap. The solution was rapidly cooled to induce gelation after which a thin layer of fluorinated non-conductive oleophobic liquid

(Fomblin Y 25/6) was added to the edge of the geometry in order to prevent evaporation at elevated temperatures. The gel was then reheated to 80 °C to fully dissolve the gel prior to starting the experiment. Temperature sweeps were performed using a cooling rate of 1 °C/min while kinetic experiments were performed by rapidly quenching (> 40 °C/min) the sample.

Scanning Transmission Electron Microscopy. Small quantities of organogels formed at 20 °C were transferred to copper grids with Formvar supports by gently touching the grid to the surface of the gel without applying pressure. Because of the thin nature of the transferred sample, the solvent evaporates rapidly under ambient conditions. Scanning transmission electron microscopy (sTEM) images were obtained with a FEI Technai G2 F20 transmission electron microscope operating at 200 kV.

RESULTS & DISCUSSION:

Self-Assembly of P3ATs in Solvent Mixtures

Self-assembly in solution for conjugated polymers is driven by a reduction in solubility induced through changes in temperature or the addition of a miscible poor-solvent.[4, 31-33] Variability in shape and structure are common for different conjugated polymers assembled in solution.[3, 4, 11, 12, 16, 18, 21, 34-37] This is largely dependent on the specific chemistry of the backbone and side chains, the regioregularity, molecular weight and the solvent environment during crystallization. Self-assembled regioregular poly(3-alkylthiophene)s (RR-P3ATs) have been shown to form long fibers (a.k.a. whiskers, nanowires or ribbons) with high aspect ratio and rectangular cross-section.[31, 35, 38] When assembled at moderately high concentrations (> 5 mg/mL) these fibers will percolate to form weak interconnected organogels.[3, 4, 6-20] Figure 1 shows the evolution of mechanical properties with decreasing temperature and solubility for a 30 mg/mL P3OT solution.

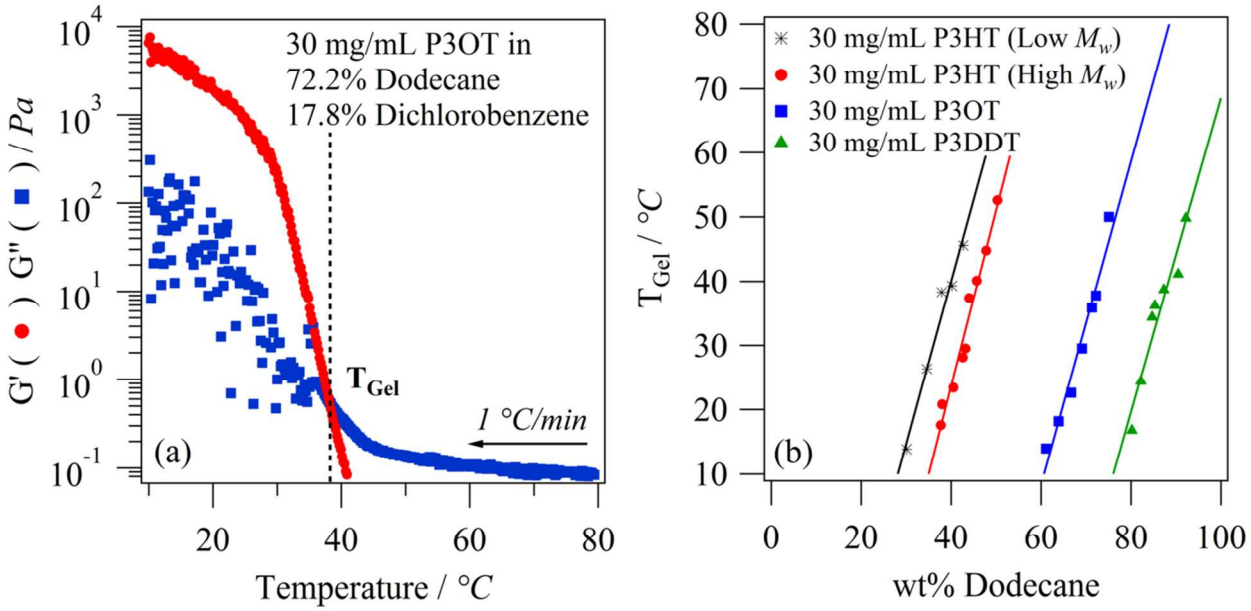

Figure 1. a) Oscillatory rheology of 30 mg/mL P3OT in a mixed solvent of dodecane/1,2-dichlorobenzene that is cooled at a rate of 1 °C/min. The gelation temperature (T_{Gel}) is defined as the crossover between the storage (G') and loss (G'') moduli. b) Gelation temperature is plotted against dodecane content in the solvent mixture for different P3ATs (all measured at a cooling rate of 1 °C/min). Linear fits are also shown with nearly identical slopes.

Figure 1a shows the rheological response of a typical P3AT in solution during a slow cooling ramp (1 °C/min). At high temperatures the solution is liquid-like ($G' = 0$). When the temperature is reduced, crystallization is eventually triggered and an elastic response is measured ($0 < G' < G''$) due to the growth of polymer fibers in solution.[12] Further cooling results in an increasing storage modulus (elastic) that eventually surpasses the loss modulus (viscous) at the crossover point ($G' = G''$). This is commonly known as the gel point because it corresponds well with mechanical percolation and gelation. The temperature corresponding to the crossover point is herein referred to as the gelation temperature (T_{Gel}). P3AT self-assembly is both a kinetic and thermodynamic process and therefore T_{Gel} will be dependent on experimental conditions such as

the cooling rate. In this work, the cooling rate was held constant for all samples but its effect is further explained in the Supporting Information (Figure S1).

Figure 1b shows that T_{Gel} varies linearly as a function of dodecane content for each alkyl chain length when all experimental conditions are held constant. Dodecane acts as a poor-solvent for P3ATs while 1,2-dichlorobenzene (DCB) acts as a "good" solvent. Therefore, it is expected that an increasing dodecane ratio would result in reduced solubility, higher gelation temperatures and faster self-assembly. The trend with alkyl chain length is also as expected. Alkyl side chains are considered detrimental to device performance because they act as electrical insulators and because they can prevent crystalline packing due to steric effects.[39, 40] Yet, they are necessary to entropically facilitate the dissolution of the typically rigid polymer backbones of conjugated polymers.[41, 42] Longer alkyl chains (e.g. P3DDT) add more entropy and result in higher polymer solubility than short alkyl chain lengths (e.g. P3HT).

Figure 1b also shows a difference in solubility between P3HT batches. In this case, it is likely as a result of differences in regioregularity (Table 1). Conjugated polymers with higher regioregularity will result in reduced solubility due to the increased stiffness of the chain and therefore gelation at lower poor solvent ratios.[43] The difference in solubility could also be the results of differences in molecular weight. However, this would be expected to produce the opposite trend where higher M_w are generally less soluble. Differences in the gelation of P3HT batches could also be the results of differences in the kinetics of self-assembly for high and low M_w P3HT, where lower M_w chains may assemble more rapidly than high M_w chains. There is also an unexpected, but distinctly linear, trend between dodecane content and gelation temperature for all P3ATs. The slopes are similar: low M_w P3HT (253 ± 24 °C/dodecane wt%), high M_w P3HT (274 ± 19 °C/dodecane wt%), P3OT (251 ± 22 °C/dodecane wt%) and P3DDT

(244 ± 31 °C/dodecane wt%) suggesting that dodecane content may influence the solubility of the thiophene backbone by changing the solvent's polarizability. This suggests that solvent mixtures and variable alkyl chain structures may help to probe for specific solvent-polymer interactions.

Solvent ratios can also be chosen to achieve similar self-assembly conditions. By using T_{Gel} as a surrogate for solubility, a solvent ratio can be chosen for each polymer to provide similar gelation conditions. We have previously shown that the network structure and properties of P3HT organogels can be modified by changes in gelation kinetics under isothermal conditions.[11] Engineering similar gelation kinetics through tunable solvent ratios allows for the study of developing structure-property relationships as a function of alkyl chain length. The nanoscale structure and electronic properties at intermediate stages of self-assembly can be studied using a combination of small angle neutron scattering (SANS) and AC dielectric spectroscopy.[12] Figure 2 shows SANS profiles and fit results, using the parallelepiped model to account for fibers and a polymer model to account for dissolved chains, for a P3HT organogel assembled isothermally at a temperature ($T_{Experiment}$) that is 5 °C lower than T_{Gel}.

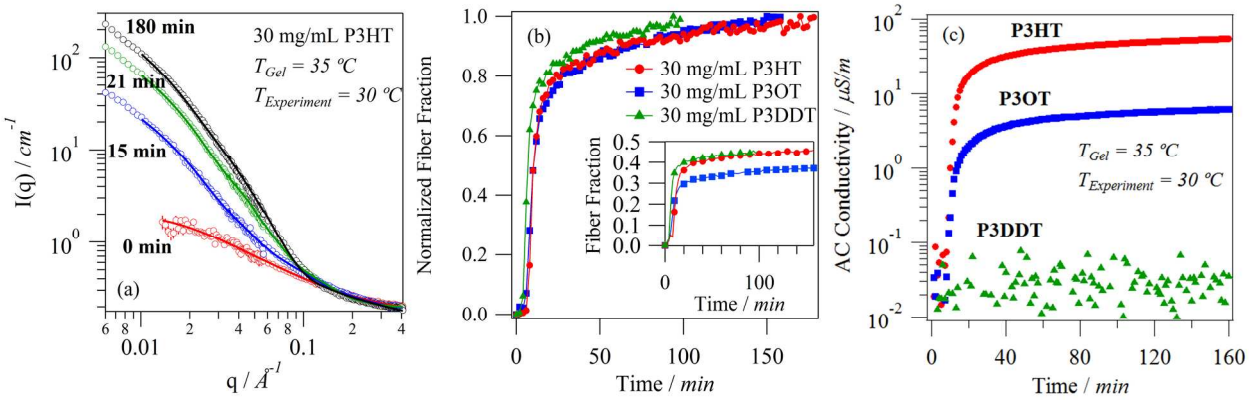

Figure 2. a) 1D SANS profiles of 30 mg/mL high M_w P3HT in 43.9% dodecane/56.1% DCB isothermally gelled at 30 °C shown at incremental times. Solid lines represent fits with a mass

balanced parallelepiped model and polymer model with excluded volume effects.[11, 12] b) Fraction of P3AT in fiber extracted from a SANS model fit for 30 mg/mL high M_w P3HT in 43.9 wt% dodecane/56.1 wt% DCB, 30 mg/mL P3OT in 71.3 wt% dodecane/28.7 wt% DCB and 30 mg/mL P3DDT in 84.7 wt% dodecane/15.3 wt% DCB, normalized to the maximum fiber fraction. The inset image shows the non-normalized fiber fraction as a function of time. c) AC conductivity (2 kHz) from simultaneous dielectric-SANS experiments for 30 mg/mL P3ATs in the same solvent mixtures as listed above.

Figure 2 shows dielectric-SANS results for 30 mg/mL P3AT organogels self-assembled in solvent mixtures. Solvent mixtures were selected for each polymer to achieve a T_{Gel} of 35 °C. This corresponded to 43.9 wt% dodecane/56.1 wt% DCB for P3HT (high M_w), 71.3 wt% dodecane/28.7 wt% DCB for P3OT and 84.7 wt% dodecane/15.3 wt% DCB for P3DDT based on Figure 1. A lower temperature ($T_{Experiment}$) of 30 °C was selected for isothermal gelation to drive the self-assembly. The measurements follow the structural evolution of samples from fully dissolved polymer to fully formed organogels.

Figure 2a shows SANS profiles fit with a mass balanced model to account for all scattering objects in solution at any point in time. Dissolved P3AT chains are represented by a model for polymers with excluded volume effects ($P_{PExV}(q)$).[11, 12, 44] P3AT fibers with rectangular cross-section are modeled using a parallelepipedon ($P_{PP}(q)$) form factor.[4, 11, 12, 19, 45] This combined model applies a mass balance on P3AT, that is limited by the total volume fraction of polymer in solution (ϕ_v), to determine the cross-sectional dimensions of the growing fibers (a and b) and to account for the fraction of P3AT that exists in fiber form (Ψ_f) at any given time. Equation 2 describes the scattering intensity (I) as a function of the scattering vector (q) for the model:

$$I(q) = \phi_v \psi_f (\Delta\rho_{PP})^2 P_{PP}(q) + \phi_v (1-\psi_f)(\Delta\rho_{PExV})^2 P_{PExV}(q) \quad (2)$$

where $\Delta\rho_{PP}$ is the scattering contrast between the solvent mixture and P3AT fibers and $\Delta\rho_{PExV}$ is the scattering contrast between the solvent mixture and the dissolved P3AT chains.[11, 12] The details of the form factor models and fit constants can be found in the Supporting Information.

By fixing most variables in the model (Equation 2) to known or independently measured values, only three unknown parameters remain: fraction of polymer in fiber from (Ψ_f), fiber thickness (*a*) and fiber width (*b*). Each profile is fit with this model enabling the accurate extraction of these parameters as a function of time. Previous studies have shown that the parallelepiped model is only valid over a limited *q*-range ($q > 0.009$ Å^{-1}) because the branched network starts to dominate the scattering at low-*q* ($q < 0.009$ Å^{-1}).[4, 11, 12] Surprisingly, the dimensions of the near-equilibrium P3AT fibers are similar. SANS shows high M_w P3HT fibers with an average width of 23.4 nm and thickness of 4.4 nm, P3OT fibers with an average width of 26.1 nm and thickness of 4.6 nm, and P3DDT fiber with an average width of 22.2 nm and thickness of 4.9 nm. The lattice parameters of non-intercalating P3AT fibers can be used to estimate that high *Mw* P3HT and P3OT fibers are on average between 2 – 3 chains thick, while P3DDT fibers are on average 2 chains thick.[26]

Figure 2b shows the kinetics of self-assembly for P3AT gels by plotting the normalized fiber fraction (Ψ_f) over time. It shows that kinetically, the gels form in a very similar fashion where almost 80% of self-assembly occurs within the first 30 minutes and then reduces to a much slower rate. The similar self-assembly kinetics for variable alkyl chain lengths indicates that the driving force is also similar. Even though the driving force for self-assembly is similar, the final conductivity of the gels varies by orders of magnitude (Figure 2c). Furthermore, the conductivity of the P3DDT sample does not change during self-assembly. The simultaneous

nature of the dielectric-SANS measurement allows for direct comparison of variations in conductivity and fiber fraction, as seen in Figure 3.

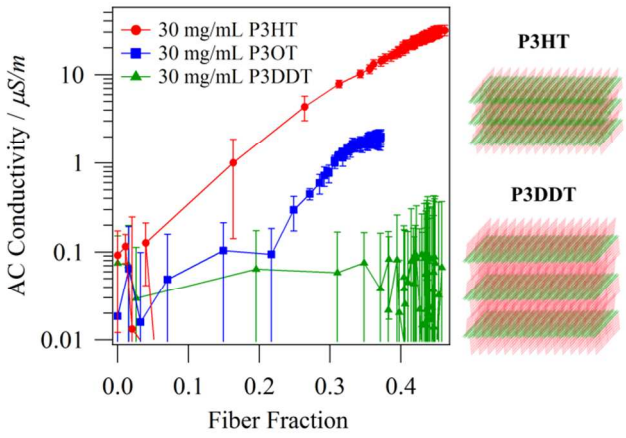

Figure 3. Variation of AC conductivity (2 kHz) with fiber fraction from isothermal dielectric-SANS at 30 °C for high M_w P3HT in 43.9% dodecane/56.1% DCB, P3OT in 71.3% dodecane/28.7% DCB and P3DDT in 84.7% dodecane/15.3% DCB. The right-set images depict the non-intercalated packing of P3HT and P3DDT fibers with the alkyl chains colored red and thiophene backbones colored green. All samples are at 30 mg/mL.

Figure 3 shows a time-based point-by-point matching of conductivity and fiber fraction. Even though self-assembly kinetics are nearly identical, as shown in Figure 2b, variations in fiber-conductivity are drastically different. P3HT gelation shows an exponential dependence between fiber fraction and conductivity for $\Psi_f > 0.04$, where increasing fibers result in a consistent increase in conductivity. P3OT self-assembly shows no significant increase in conductivity for $\Psi_f < 0.21$ at which point there is a rapid increase in conductivity with new fiber formation ($0.21 < \Psi_f < 0.34$) followed by a plateau in conductivity ($\Psi_f > 0.34$). In contrast, P3DDT shows no increase in conductivity upon the formation of new fibers. The differences in magnitude of the conductivity at similar fiber fractions are likely due, in part, to

the difference in alkyl chain length. The right-set image in Figure 3 contrasts three chain stacks of fiber cross-sections for P3HT and P3DDT. The conjugated thiophene backbone is colored green while the insulating alkyl chains are colored red. It is obvious that charge hoping between thiophene layers, a transport mechanism in conjugated polymer networks, will be less likely for longer alkyl chains.[46] This may also explain the shift in fiber percolation threshold for these gels where P3HT is Ψ_f ~ 0.04, P3OT is Ψ_f ~ 0.21. For P3DDT the changes in conductivity are either below the resolution of the measurement or even more fibers would be needed to achieve percolation (i.e. $\Psi_f > 0.48$).

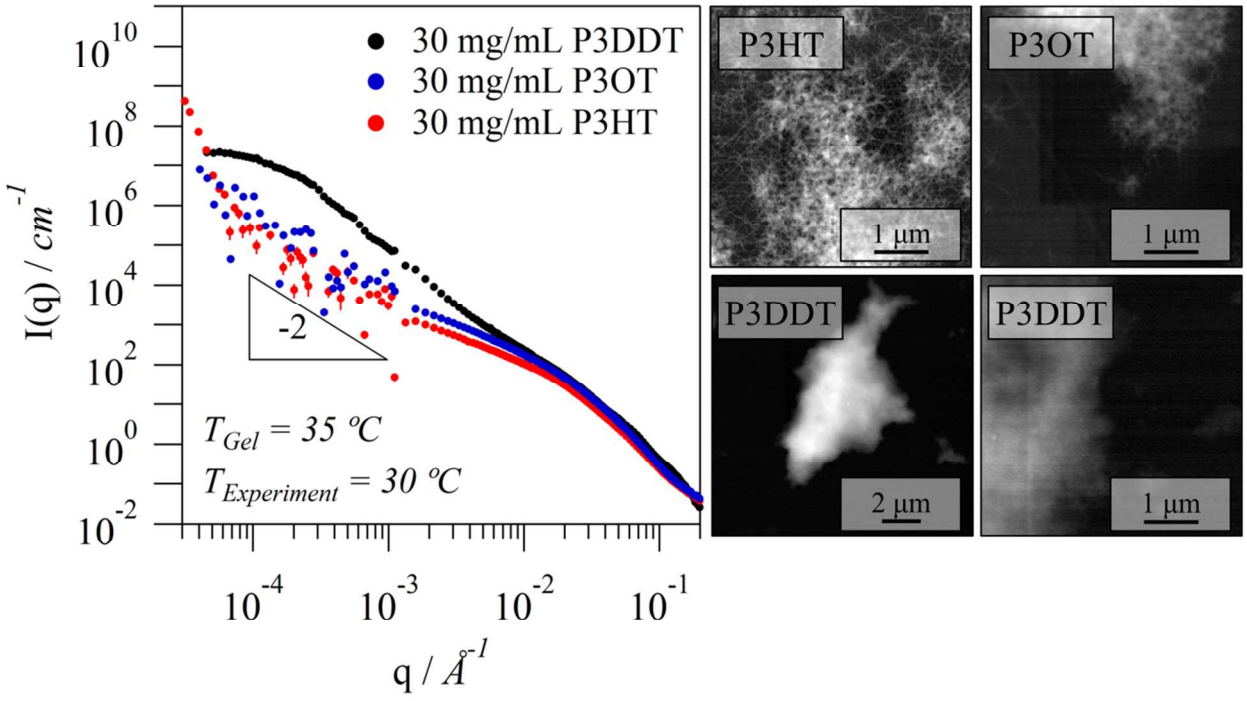

Figure 4. Left: Combined SANS and USANS (desmeared) profiles of high M_w P3HT in 43.9% dodecane/56.1% DCB, P3OT in 71.3% dodecane/28.7% DCB and P3DDT in 84.7% dodecane/15.3% DCB self-assembled for 24 hours at 30 °C. Right: Corresponding sTEM images of dried P3AT organogels self-assembled at the same solvent ratios. All samples are at 30 mg/mL.

Figure 4 shows that scattering profiles at high-q ($q > 0.009$ Å^{-1}) are similar in the region corresponding to the fiber cross-sectional dimensions. In contrast, the scattering at $q < 0.009$ Å^{-1} is sometimes quite different. We attribute this to differences in inter-fiber correlations due to the formation of networks that lead to a power-law dependence that is larger than that expected for isolated rigid fibers (q^{-1}).[4, 11, 12, 21, 47] Figure 4 clearly shows that P3HT and P3OT have very similar network features over a range of $10^{-4} < q$ (Å^{-1}) $< 10^{-2}$, corresponding to real space dimensions of 63 nm – 6.3 μm. This observation is also consistent with sTEM images (Figure 4), showing that networks for both samples are similar, having clearly defined fibers as well as regions of higher and lower fiber densities. In contrast, the scattering profile of the P3DDT gel at low q (USANS range) is significantly different and has larger slope (i.e. approaching -2) that is suggestive of a denser network. It also shows a clear turnover that is characteristic of finite domains with a characteristic feature size (radius of gyration) of approximately 1.2 μm based on a Guinier fit.[4, 11] The Guinier equation is chosen as the simplest model to quantify the size of isolated high fiber density domains that are dispersed in a lower density matrix. Moreover, the characteristic length scale obtained from SANS/USANS corresponds well with the observed size of dense fiber regions (sTEM) that are dispersed within a homogeneous mixture of solvent (> 96% v/v) and fibers. The smaller characteristic size and the lower level of order found in these heterogeneous P3DDT domains, in combination with the long insulating alkyl chains, most likely lead to the low bulk conductivities that are observed in Figure 3. At even lower angles, $q < 10^{-4}$ Å^{-1}, the scattering of P3HT and P3OT also start to differ. The profile of the P3OT organogel has a fairly constant slope at low q but there is a turn-over to a larger slope for the P3HT organogel. This is suggestive of a slightly more heterogeneous network structure for P3HT organogels when compared to P3OT for the largest length scales (> 10 μm).[4, 11] The similarity

between P3HT and P3OT at all other length scales suggests that the dependence of conductivity (Figure 3) in these samples is most likely dominated by the length of the insulating alkyl chains.

The self-assembly mechanism is similar for P3ATs of differing alkyl chains (Figure 1). However, it is found that similar self-assembly kinetics (Figure 2) do not necessarily produce identical fiber and network structures, as shown in Figure 4. When similar network structures are produced, as in the case of P3HT and P3OT gels, the length of the alkyl chain is likely the dominating attribute that leads to differences in bulk conductivity.

Structure-Property Engineering through Solvent Mixtures

Figures 3 & 4 demonstrate that differences in structure can lead to drastic differences in bulk conductivity values. Therefore, in order to optimize electronic properties of organogels from a specific polymeric material, it is first necessary to manipulate the structure of the networks that are formed. One route towards modifying network structures is to change the rate of aggregation through variations in solvent quality for any given polymer-solvent mixture. The theory that links gelation kinetics to supersaturation and to network structure has been established by Li *et al.*[48] Generally, larger supersaturation levels lead to more nucleation centers and to more frequent stacking mistakes so that the resulting networks are more densely branched and heterogeneous. De la Iglesia and coworkers recently reported that, for organogels of poly(9,9-dioctylfluorine) (PFO), increased supersaturation results in denser and more highly-branched networks.[21] Figure 5 shows a schematic of the expected trends and sTEM images of low M_w P3HT organogel networks formed in different good-solvent/poor-solvent mixtures to modify the supersaturation levels. This figure demonstrates that low M_w P3HT organogels form fibrillar networks with variable fiber density. Unforntunately, structural features from sTEM images are difficult to quantify for P3AT organogels due to the potential for fiber aggregation

during drying as well as convoltution from film thickness variations. Fitting results from SANS experimeriments, as seen in Figure 6, provide a more accurate quantification of structural differences in organogels.

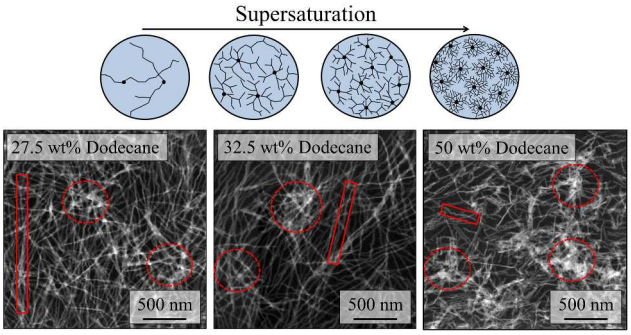

Figure 5. Top: Schematics showing the correlation between solvent-quality and fiber branching as proposed by Li *et al*.[48] Bottom: Scanning transmission electron microscopy (sTEM) images of 30 mg/mL low M_w P3HT organogels isothermally self-assembled to equilibrium in 1,2-dichlorobenzene/dodecane solvent mixtures at 20 °C. Samples were allowed to evaporate prior to imaging. Fiber length is highlighted with a solid box and dense fiber regions are highlighted with a dashed circle.

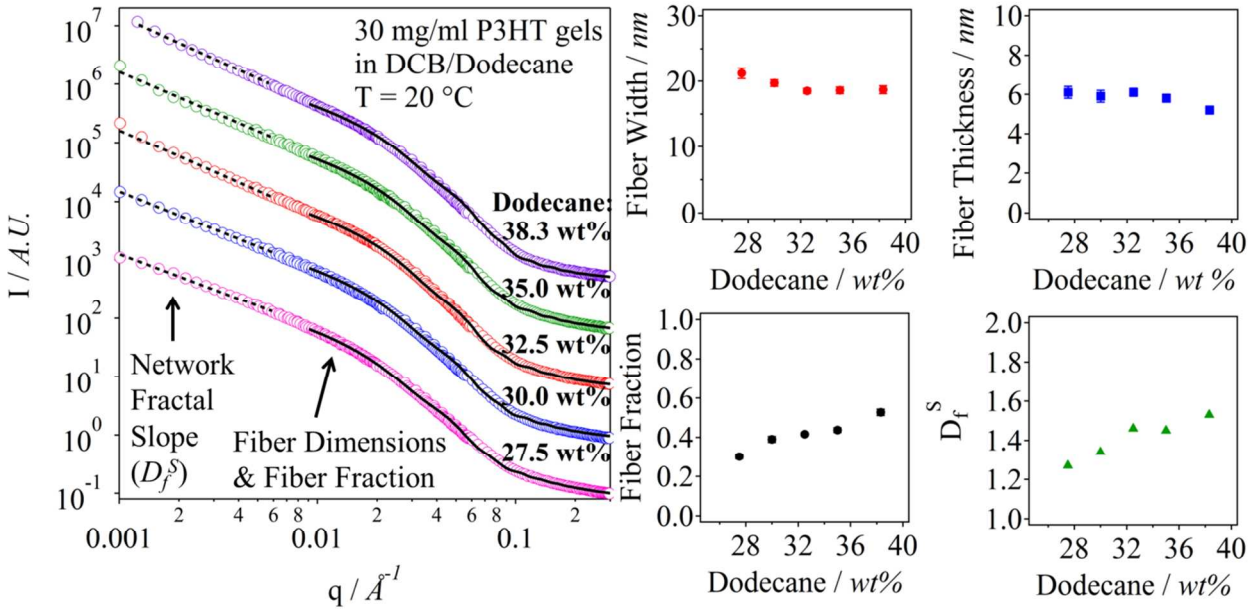

Figure 6. SANS profiles and corresponding fits, both shifted for clarity, of 30 mg/mL low M_w P3HT in dodecane/1,2-dichlorobenzene solvent mixtures self-assembled for at least 24 hours at 20 °C. Fiber width, fiber thickness and fiber fraction are extracted from SANS using Equation 2. The network fractal dimension (D_f^S) is extracted using a power law fit of the SANS profiles from $0.001 < q$ (Å^{-1}) < 0.006 shown as a dashed black line.

Figure 6 shows the SANS profiles, fit with Equation 2, of fully formed low M_w P3HT organogels formed in mixtures of 1,2-dichlorobenzene and dodecane (i.e. good-solvent/poor-solvent) at different ratios. As previously demonstrated, changes in driving force for P3HT organogel self-assembly have little impact on the cross-sectional shape of the fibers.[11] In this case, the fiber thickness and width are nearly identical with an average width of ~20 nm, consistent with sTEM images (Figure 5), and an average thickness of ~6 nm that corresponds to three polymer chains after assuming no interdigitation of side-chains.[26] Figure 6 also shows that more fibers are formed as a result of increasing the dodecane content. This trend is expected because increasing dodecane (i.e. poor solvent) should lead to a higher driving force for self-assembly.

At low-q ($q < 0.006$ Å^{-1}), SANS profiles are also fit with a power law equation to extract fractal dimension (D_f^S) values. Fractal behavior in fiber gels originate from inter-fiber correlations that develop over a limited size range.[4] Although the fractal region that is shown in Figure 6 is limited to less than a decade, Figure S9 in the supplemental information combines SANS and desmeared USANS data demonstrating that it actually extends well beyond this region towards much lower q. Still, values reported in Figure 6 are from fits to only the SANS region because this data has a much smaller experimental uncertainty and because, unlike USANS, it is not significantly affected by instrumental smearing. The D_f^S values presented in

Figure 6 show a similar trend to sTEM images (Figure 5), where increasing dodecane content results in the densification of the networks. The values of the fractal dimension are D_f^S = 1.27 for low M_w P3HT in 27.5 wt% dodecane and D_f^S = 1.53 for low M_w P3HT in 38.3 wt% dodecane. The steady increase in fractal dimension correlates well with sTEM observations where the frequency of straight fibers (i.e., low branching) increases as the dodecane content decreases. Though clearly trending upwards, the change in fractal dimension is still somewhat modest (1.27 < D_f^S < 1.53) over the dodecane range (25 – 38.5 wt%) measured in SANS/USANS. More substantial differences in branching and in the size and density of the nucleation centers were observed in samples with even larger dodecane content (Figure 5) but these were, unfortunately, not characterized with SANS/USANS due to extremely rapid gelation kinetics that prevented sample loading. Moreover, although changes in the flexibility of individual fibers could also lead to changes to the power-law exponent, we primarily ascribe these to variations in the networkstructure because this is consistent with electron microscopy and because cross-sectional fiber dimensions are relatively unchanged over all solvent compositions.

Figure 7 shows the USANS profiles corresponding to some of the SANS profiles in Figure 6. This technique characterizes features over a larger size range (250 nm to 20 μm). All of the USANS profiles, except for the low M_w P3HT gel in 27.5 wt% dodecane, show a turnover at low-q that is similar to that which is observed for the P3DDT gel in Figure 4. This also suggests the formation of a more heterogeneous network (i.e., smaller and more abundant nucleation centers) as schematically depicted in the inset of Figure 7.[49, 50] The turnover is again fit to the Guinier equation to obtain a characteristic size (i.e., radius of gyration) for the heterogeneous domains. These were found to be 5.1 μm, 1.3 μm, 1.1 μm for 30 mg/mL low M_w P3HT in 30 wt%, 32.5 wt% and 38.3 wt% dodecane.

Previous work has shown that dimensions obtained from turn-overs in the USANS region for P3HT organogels (i.e. similar to those in Figure 7) correlate well with the typical size of regions observed in sTEM that had very high fiber densities.[4, 11, 12] These dense regions result in a lower local scattering length density when compared to the surrounding network and this leads to the plateau at low-*q* (USANS). These domains are presumed to be nucleation centers where large-scale fiber growth originates and proceeds through a nucleation and growth self-assembly mechanism.[11] Discrete nucleation centers form during the initial stages of self-assembly and grow until they intersect others to form a percolated network structure. The formation of a larger number of initial nuclei results in networks with smaller characteristic features and a more heterogeneous structure (Figure 5 schematic).

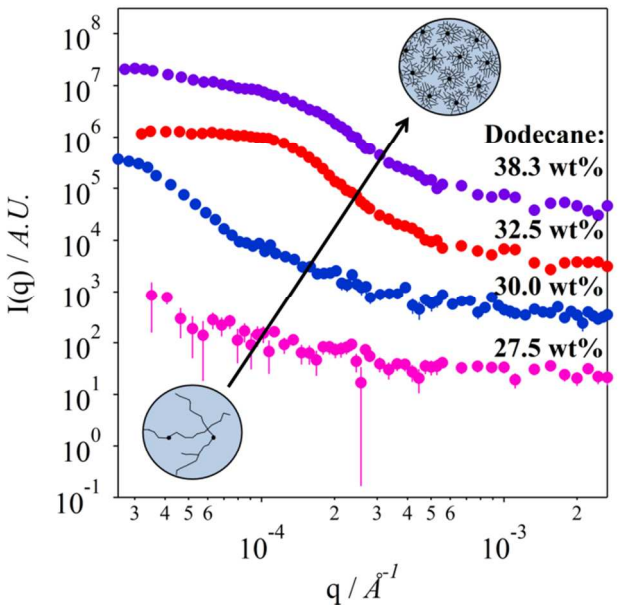

Figure 7. USANS profiles (with instrumental smearing) of 30 mg/mL low M_w P3HT in 1,2-dichlorobenzene/dodecane solvent mixtures self-assembled for at least 24 hours at 20 °C.

Kinetic behavior was also probed to investigate the potential for modifying bulk viscoelastic and electronic properties by using solvent mixtures to tune supersaturation during

self-assembly. Figure 8 shows isothermal gelation rheology for P3HT organogels formed in different solvent mixture ratios. The complex modulus (G^*), where $G^*=\sqrt{(G')^2+(G'')^2}$, is plotted as a function of time after the temperature reaches 20 °C. Similar to the results shown in Figure 2c, all samples start as viscous polymer solutions before the modulus rapidly increases indicating gelation. The initial gelation time decreases as the fraction of dodecane increases. Furthermore, the final modulus of the gel steadily increases with increasing poor-solvent for samples in the range of 25 – 30 wt% dodecane. Interestingly, the final modulus of samples with an excess of 30 wt% dodecane decreases again. This same trend is observed in the final conductivity of the P3AT organogels (Figure 9). A maximum in conductivity was also observed by Zhu and coworkers who studied P3HT solution phase self-assembly using solvent mixtures (chlorobenzene/anisole), but they could not relate this to the changing structures.[37] Data from SANS, USANS and sTEM all suggest that moduli and conductivity maxima are a result of competing factors between increasing fiber fractions and increasing network heterogeneity (i.e., more abundant and smaller nucleation centers). Gels formed at low dodecane fractions form fewer fibers (Figure 6) and fewer nucleation centers leading to a more homogeneous structure (Figures 7). In contrast, gels with high dodecane content contain more fibers (Figure 6) but also have large numbers of nucleation centers (Figure 7) that lead to a more heterogeneous and disordered network with poor-quality inter-fiber connections. This leads to a maximum conductivity due to the competition of having networks with large fibers content (favored by high supersaturation) and also homogeneous structures with long and highly ordered fibers (favored by low supersaturation). Difference in conductivities (Figure 9) of more than order of magnitude are achieved for organogels that have identical types and concentrations of conjugated

polymer. This demonstrates that solvent mixtures are important engineering parameters to optimize the performance and structure of networks in organic electronic devices.

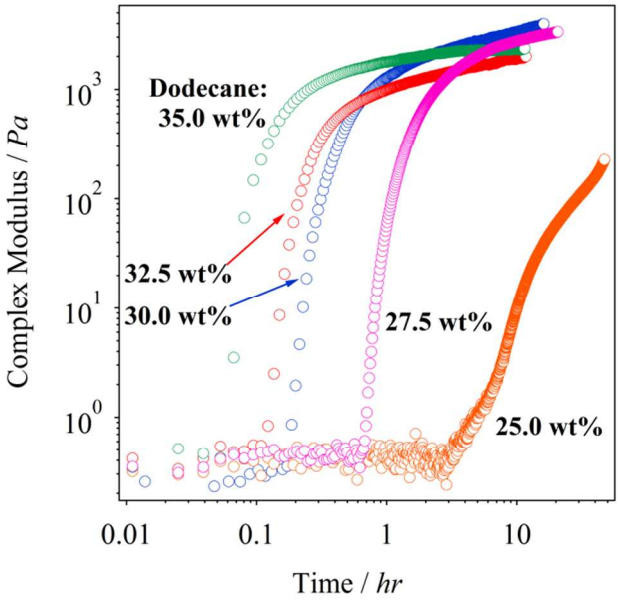

Figure 8. Oscillatory rheology of 30 mg/mL low M_w P3HT in 1,2-dichlorobenzene/dodecane solvent mixtures during isothermal gelation at 20 °C.

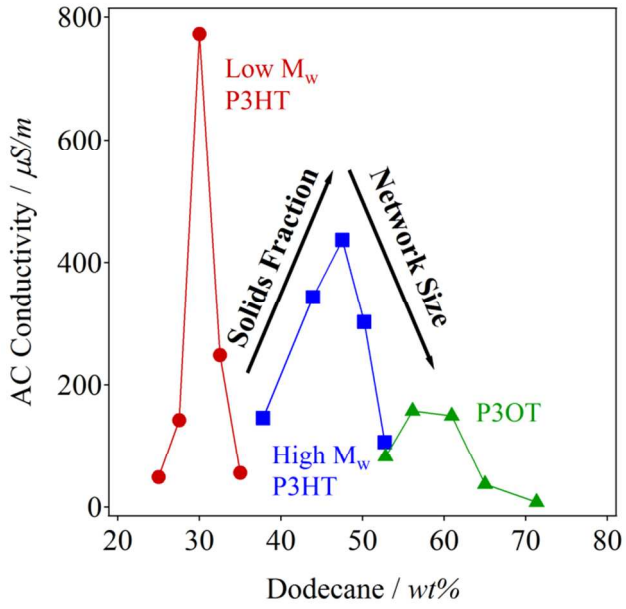

Figure 9. AC conductivity (2 kHz) of 30 mg/mL low M_w P3HT, high M_w P3HT and P3OT organogels self-assembled to equilibrium at 20 °C in 1,2-dichlorobenzene/dodecane solvent mixtures.

Thermoreversible Gelation in Thin-Films

Results presented so far demonstrate the possibility of engineering the structure of bulk P3AT organogels over multiple length scales through variations in the solvent/non-solvent ratio and/or alkyl chain length. Yet, bulk organogels are not very useful in organic electronic applications where active layer materials are usually coated from solution for efficient and economic processing. Therefore, it is also necessary to demonstrate that organogel materials can be designed for large-scale continuous processing (e.g. roll-to-roll). Processing interconnected networks for thin-film organic electronics has been previously suggested but elastic properties (Figure 8) are generally incompatible with traditional coating processes (e.g. spin-coating).[22]

Here, a solvent/poor-solvent pair with very low-volatility is used to manipulate the kinetics of gelation for several P3ATs. This now creates new possibilities for structural design of conjugated polymer organogels for deposition as films (thick or thin) through the use of similar engineering principles. The pictures in Figure 10 compare thermoreversible gelation in the bulk and in thin-films for P3HT. The formation of organogel thin-films after deposition from a liquid state is possible because the vapor pressures of the two solvents are low enough to stop evaporation so that gelation can reach completion. The vapor pressure of 1,2-dichlorobenzene (DCB) is only 1.4 mm Hg at 20 °C and that of n-dodecane is only 0.1 mm Hg at 20 °C.[51] At sufficiently high temperatures, a fully dissolved sample (bright orange) is deposited as a liquid using traditional coating processes. When the temperature is reduced, usually upon contact with the substrate, the material starts to form a gel over a period of time that can be manipulated by

changing the solvent/poor-solvent content (Figure 10). If re-heated, the gels will fully re-dissolve and form a bright orange polymer solution. The thermo-reversible nature of the thin film indicates that the solvent is still entrained in the polymer as a result of gelation. The solvent can be removed with vacuum over approximately 24 hours or, more effectively, by rinsing films in a miscible poor-solvent of higher volatility (e.g. hexane) after the gel is fully formed. The films shown in Figure 10 were produced using drop-casting but we have also used blade coating, screen printing and spin coating to successfully deposit organogel materials. Despite this successful demonstration, it is very likely that self-assembly in tightly confined films will not produce identical structures to those reported here for bulk samples. Future experiments should focus on developing structure-property relationships for organogels that are formed under confinement.

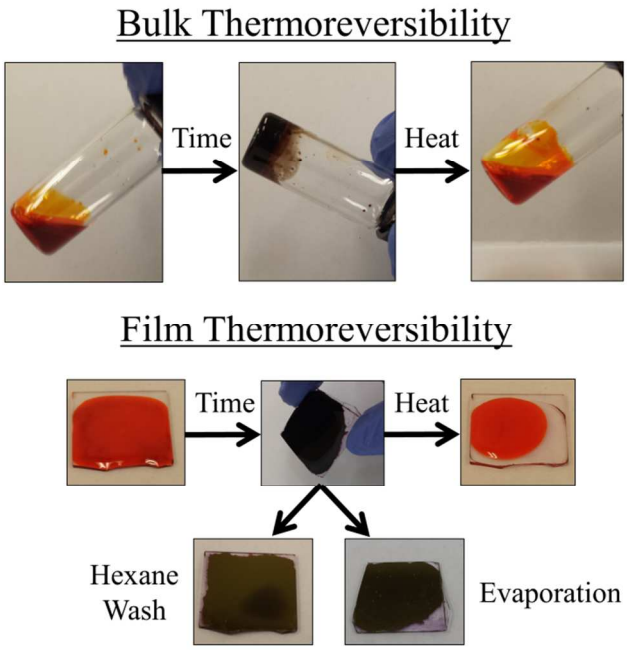

Figure 10. Photographs of a 30 mg/mL low M_w P3HT in a solvent mixture of 30% dodecane and 70 wt% 1,2-dichlorobenzene. Top images represent bulk gelation while bottom images represent gels formed in a film. The left images, on both the top and bottom sections, correspond to a fully

dissolved P3HT solution after heating. Over time the samples, in bulk or in a film, self-assemble into P3HT organogels that can be re-heated to re-dissolve the gel. The two lower images correspond to organogel films after drying under vacuum or through a hexane wash.

CONCLUSIONS:

It has been demonstrated that low volatility solvent/poor-solvent mixtures can be used to engineer the structure and properties of poly(3-alkylthiophene) (P3AT) organogels. Furthermore, it is also shown that low-volatility solvent mixtures allow processing of samples as liquids to eventually form organogel films via self-assembly. Organogels of conjugated polymers with desired structure and properties could be optimized for use in organic electronics. The use of dodecane and 1,2-dichlorobenzene mixtures as a universal solvent system permitted the gelation of P3AT polymers with a wide range of alkyl chain lengths. Differences in alkyl chain length led to drastically different properties even when self-assembly kinetics were similar. Increasing dodecane fraction leads to faster self-assembly kinetics for P3HT organogels due to a larger driving force. sTEM, SANS and USANS all show that higher dodecane content leads to more branching and smaller network features. A peak in the conductivity of several different P3AT gels was found due to a competition between increasing the total number of fibers and decreasing the size of the network features (i.e. nucleation centers), both of which were affected by the dodecane content. These results demonstrate that simple and tunable parameters, such as alkyl chain structure and solvent/poor-solvent content, can lead to large variations in properties of conjugated polymer organogels. Moreover, the work also presents a novel approach to incorporate this engineering control into thin-film electronic device applications.

ACKNOWLEDGEMENTS:

This material is based upon work supported by the U.S. Department of Energy, Office of Science, Office of Basic Energy Science under award number DE-SC0005153. We acknowledge the support of the National Institute of Standards and Technology, U.S. Department of Commerce, in providing the neutron research facilities used in the work. This work utilized facilities supported in part by the National Science Foundation under Agreement No. DMR-0944772. This work benefitted from DANSE software developed under NSF award DMR-0520547. Part of this work was conducted at the University of Washington NanoTech User Facility, a member of the NSF National Nanotechnology Infrastructure Network (NNIN).

Electronic Supplementary Information (ESI): Organogel rheology kinetics, SANS fitting procedure and full AC dielectric spectrum during P3AT self-assembly.

REFERENCES:

1. K. Coakley and M. McGehee, *Chemistry of Materials*, 2004, **16**, 4533-4542.
2. H. Hoppe and N. Sariciftci, *Journal of Materials Research*, 2004, **19**, 1924-1945.
3. F. S. Kim and S. A. Jenekhe, *Macromolecules*, 2012, **45**, 7514-7519.
4. G. M. Newbloom, F. S. Kim, S. A. Jenekhe and D. C. Pozzo, *Macromolecules*, 2011, **44**, 3801-3809.
5. W. Yin and M. Dadmun, *ACS Nano*, 2011, **5**, 4756-4768.
6. J.-Y. Chen, F.-C. Hsu, Y.-M. Sung and Y.-F. Chen, *Journal of Materials Chemistry*, 2012, **22**, 15726-15731.
7. P.-T. Huang, Y.-S. Chang and C.-W. Chou, *Journal of Applied Polymer Science*, 2011, **122**, 233-240.
8. W. Y. Huang, P. T. Huang, Y. K. Han, C. C. Lee, T. L. Hsieh and M. Y. Chang, *Macromolecules*, 2008, **41**, 7485-7489.

9. S. Malik, T. Jana and A. K. Nandi, *Macromolecules*, 2001, **34**, 275-282.

10. S. Malik and A. K. Nandi, *Journal of Physical Chemistry B*, 2004, **108**, 597-604.

11. G. M. Newbloom, K. M. Weigandt and D. C. Pozzo, *Macromolecules*, 2012, **45**, 3452-3462.

12. G. M. Newbloom, K. M. Weigandt and D. C. Pozzo, *Soft Matter*, 2012, **8**, 8854-8864.

13. M. J. Sobkowicz, R. L. Jones, R. J. Kline and D. M. DeLongchamp, *Macromolecules*, 2011, **45**, 1046-1055.

14. W. Xu, L. Li, H. Tang, H. Li, X. Zhao and X. Yang, *The Journal of Physical Chemistry B*, 2011, **115**, 6412-6420.

15. W. Xu, H. Tang, H. Lv, J. Li, X. Zhao, H. Li, N. Wang and X. Yang, *Soft Matter*, 2012, **8**, 726-733.

16. S. Berson, R. De Bettignies, S. Bailly and S. Guillerez, *Advanced Functional Materials*, 2007, **17**, 1377-1384.

17. M.-Y. Chang, Y.-H. Huang and Y.-K. Han, *Organic Electronics*, 2014, **15**, 251-259.

18. Z. Yu, J. Fang, H. Yan, Y. Zhang, K. Lu and Z. Wei, *The Journal of Physical Chemistry C*, 2012, **116**, 23858-23863.

19. J. K. Keum, K. Xiao, I. N. Ivanov, K. Hong, J. F. Browning, G. S. Smith, M. Shao, K. C. Littrell, A. J. Rondinone, E. Andrew Payzant, J. Chen and D. K. Hensley, *CrystEngComm*, 2013, **15**, 1114-1124.

20. N. Seidler, G. M. Lazzerini, G. L. Destri, G. Marletta and F. Cacialli, *Journal of Materials Chemistry C*, 2013, **1**, 7748-7757.

21. P. de la Iglesia and D. C. Pozzo, *Soft Matter*, 2013, **9**, 11214-11224.

22. M. Koppe, C. Brabec, S. Heiml, A. Schausberger, W. Duffy, M. Heeney and I. McCulloch, *Macromolecules*, 2009, **42**, 4661-4666.

23. J. J. Richards, K. M. Weigandt and D. C. Pozzo, *Journal of Colloid and Interface Science*, 2011, **364**, 341-350.

24. B.-G. Kim, E. J. Jeong, H. J. Park, D. Bilby, L. J. Guo and J. Kim, *ACS Applied Materials & Interfaces*, 2011, **3**, 674-680.

25. M. Brinkmann and J. C. Wittmann, *Advanced Materials*, 2006, **18**, 860-863.

26. T. J. Prosa, M. J. Winokur, J. Moulton, P. Smith and A. J. Heeger, *Macromolecules*, 1992, **25**, 4364-4372.

27. C. Glinka, J. Barker, B. Hammouda, S. Krueger, J. Moyer and W. Orts, *Journal of Applied Crystallography*, 1998, **31**, 430-445.

28. S. Kline, *Journal of Applied Crystallography*, 2006, **39**, 895-900.

29. J. G. Barker, C. J. Glinka, J. J. Moyer, M. H. Kim, A. R. Drews and M. Agamalian, *Journal of Applied Crystallography*, 2005, **38**, 1004-1011.

30. P. Butler, G. Alina, R. C. Hernandez, M. Doucet, A. Jackson, P. Kienzle, S. Kline and J. Zhou, SASView for Small Angle Scattering Analysis, http://www.sasview.org/.

31. W. D. Oosterbaan, J.-C. Bolsée, A. Gadisa, V. Vrindts, S. Bertho, J. D'Haen, T. J. Cleij, L. Lutsen, C. R. McNeill, L. Thomsen, J. V. Manca and D. Vanderzande, *Advanced Functional Materials*, 2010, **20**, 792-802.

32. S. Samitsu, T. Shimomura, S. Heike, T. Hashizume and K. Ito, *Macromolecules*, 2008, **41**, 8000-8010.

33. S. Samitsu, T. Shimomura and K. Ito, *Thin Solid Films*, 2008, **516**, 2478-2486.

34. D. Alcazar, F. Wang, T. M. Swager and E. L. Thomas, *Macromolecules*, 2008, **41**, 9863-9868.

35. J. Liu, M. Arif, J. Zou, S. I. Khondaker and L. Zhai, *Macromolecules*, 2009, **42**, 9390-9393.

36. C. Szymanski, C. Wu, J. Hooper, M. A. Salazar, A. Perdomo, A. Dukes and J. McNeill, *The Journal of Physical Chemistry B*, 2005, **109**, 8543-8546.

37. Z. Zhu, B. Wei and J. Wang, *physica status solidi (RRL) – Rapid Research Letters*, 2013, **8**, 252-255.

38. S. Samitsu, T. Shimomura, S. Heike, T. Hashizume and K. Ito, *Macromolecules*, 2010, **43**, 7891-7894.

39. H. Sirringhaus, P. Brown, R. Friend, M. Nielsen, K. Bechgaard, B. Langeveld-Voss, A. Spiering, R. Janssen, E. Meijer, P. Herwig and D. de Leeuw, *Nature*, 1999, **401**, 685-688.

40. Y. Yao, H. Dong and W. Hu, *Polymer Chemistry*, 2013, **4**, 5197-5205.

41. M. Ballauff, *Macromolecules*, 1986, **19**, 1366-1374.

42. K. S. Schweizer, *The Journal of Chemical Physics*, 1986, **85**, 1156-1175.

43. A. Salleo, *Materials Today*, 2007, **10**, 38-45.

44. B. Hammouda, *Advances in Polymer Science*, 1993, **106**, 87-133.

45. P. Mittelbach and G. Porod, *Acta Physica Austriaca*, 1961, **14**, 185-211.

46. Y.-K. Lan and C.-I. Huang, *The Journal of Physical Chemistry B*, 2008, **112**, 14857-14862.

47. J.-L. M. Abboud and R. Notario, *Pure and Applied Chemistry*, 1999, **71**, 645-718.

48. J. L. Li, B. Yuan, X. Y. Liu and H. Y. Xu, *Crystal Growth & Design*, 2010, **10**, 2699-2706.

49. G. A. Evmenenko, T. Budtova, A. Buyanov and S. Frekel, *Polymer*, 1996, **37**, 5499-5502.

50. J. Teixeira, *Journal of Applied Crystallography*, 1988, **21**, 781-785.

51. *Handbook of Chemistry and Physics: 83rd Edition*, CRC Press LLC, Davers, MA, 2002.